

# Improvement of Photovoltaic Systems with Tracking of the Maximum Power Point in Low-Irradiation Atmospheric Conditions

Dieudonné Marcel Djanssou<sup>a, \*</sup>, Abdouramani Dadjé<sup>a, b</sup>, Fabrice Kwefeu Mbakop<sup>a, c</sup>,  
 Noël Djongyang<sup>a</sup>

<sup>a</sup> Department of Renewable Energy  
 National Advanced School of Engineering of Maroua  
 University of Maroua, Cameroon

<sup>b</sup> School of Geology and Mining Engineering  
 University of Ngaoundéré  
 Ngaoundéré, Cameroon.

<sup>c</sup> Department of Renewable Energy and Energy Performance  
 Higher Institute of Agriculture, Forestry, Water and Environment  
 University of Ebolowa  
 Ebolowa, Cameroon

## Abstract

This paper discusses the efficient use of photovoltaic energy in areas with low solar irradiation. To extract the maximum power at low irradiation, we used a maximum power point tracking (MPPT) algorithm based on the combination of fuzzy logic (FL) and the sliding mode (SM) associated with a Proportional-Integral (PI) regulator. The system parameters are calculated using the particle swarm optimization (PSO) technique, which thus ensures the stability of the controller. The performance of the proposed technique is compared with the conventional perturb and observe (P&O) technique in terms of tracking time and tracking efficiency at low irradiation. The simulation results prove that the technique has high tracking efficiency and less convergence time under low irradiation, with fewer power oscillations, low ripple and no overshoot.

**Keywords:** low irradiation, MPPT, PI regulator, fuzzy logic, PSO, sliding mode.

## I. INTRODUCTION

### Abbreviations

$V_{oc}$ : Open-circuit voltage (V)
$T_r$ : Reference temperature of the cell (K)
$T$ : Temperature of the cell (K)
$q$ : Charge of the electrons ( $1.6 \times 10^{-19}C$ )
$A$ : diode ideality factor
$E_g = 1.12[eV]$ : Band gap energy of the semiconductor (monocrystalline silicon)[1] used in the PV cell
$E$ : Solar irradiation ( $W/m^2$ )
$I_0$ : Inverse saturation current (A)
$I_{0r}$ : Inverse saturation current at $T_r$ (A)
$I$ : Current of the PV module (A)
$I_r$ : Photo-current (A)
$I_{scr}$ : Cell's short-circuit current at the reference irradiation and temperature (A)
$K$ Boltzmann's constant ( $1.3805 \times 10^{-23} J/K$ )
$K_i$ : short-circuit temperature coefficient
$N_s$ : Number of series connected cells
$N_p$ : number of parallel connected cells

Presently, merely about 18% of the global energy demand is fulfilled by renewable energy sources. Nevertheless, there exists substantial potential to enhance their contribution. Indeed, it has been approximated that the technical capacity of renewable energy surpasses the current global primary energy demand by more than 18 times [1], [2]. Among these energy sources, solar photovoltaic (PV) is of great interest. Nevertheless, a drawback of photovoltaic (PV) systems is their limited efficiency in converting solar energy into electrical energy. The energy output is significantly impacted by environmental factors, including solar radiation and temperature. Most of the literature on maximum power point tracking (MPPT) does not address its operation in low irradiation. The MPPTs developed so far have not been studied under permanently low radiation conditions. Most have taken into account the standard laboratory condition of  $1000 W/m^2$ .

In reality, the irradiation of  $1000 W/m^2$  is not always reached continuously in real-time. Researchers have developed various MPPT methods to enhance the system's efficiency and ensure it operates at the maximum power point of the photovoltaic (PV) module. The conventional MPPT perturb and observe (P&O) and increment conductance (INC) [3], [4] offer several advantages, including simplicity, low cost, easy implementation, and requiring fewer parameter measurements [5]. However, they face challenges in locating the maximum power point (MPP) under rapidly changing environmental conditions, with issues related to low convergence and oscillation of the output voltage.

\* Corresponding Author.

Email: dieudonnemarceldjanssou@gmail.com

Received: March 17, 2023 ; Revised: October 08, 2023

Accepted: November 06, 2023 ; Published: December 31, 2023

These limitations are overcome by soft computing MPPT, which comprises numerical computing and optimization, segmentation, and artificial intelligence-based methods such as the grey wolf algorithm [6], the Jaya algorithm [7], the genetic algorithm [8], the ant-colony optimization [9], neural networks (ANN), and fuzzy logic (FLC) [10]. These methods have demonstrated rapid convergence and superior performance across diverse environmental conditions compared to their conventional counterparts [3], [11]. Unfortunately, conventional MPPTs and soft computing MPPTs have not been studied in conditions of low permanent solar irradiation. Therefore, this article presents a hybrid MPPT that works optimally in conditions of low irradiation. Sliding mode control (SMC) has garnered significant attention owing to its benefits, including assured stability, resilience against parameter fluctuations, rapid dynamic response, and ease of implementation. This approach combines artificial intelligence with robustness to deliver optimal performance [12]. In this method, fuzzy logic is employed to generate the reference voltage at maximum power. Subsequently, sliding mode control (SMC) is utilized to minimize the error between the voltages of the photovoltaic generator and generate the precise duty cycle for the DC-DC converter, ensuring the generator operates at its maximum power. The gain parameters are optimized by particle swarm optimization (PSO) to ensure system stability and reduce oscillation. The application of the PSO technique to adjust the parameters of the SMC-PI controller enhances the response by ensuring stability and minimizing oscillations, all without the need for intricate mathematical analysis. The rest of this work is organized as follows: Section 2 outlines the suggested procedure, and the diverse outcomes are detailed in Part 3 Section 2. Section 3 concludes the discussion.

## II. MATERIALS AND METHODS

### A. Materials

#### 1) Modelling and control of the photovoltaic system

The entire PV system with the MPPT controller is developed within the Matlab/SIMULINK environment. The simulated PV system is depicted in Figure 3. Figure 1 comprises a PV generator, an MPPT containing a boost

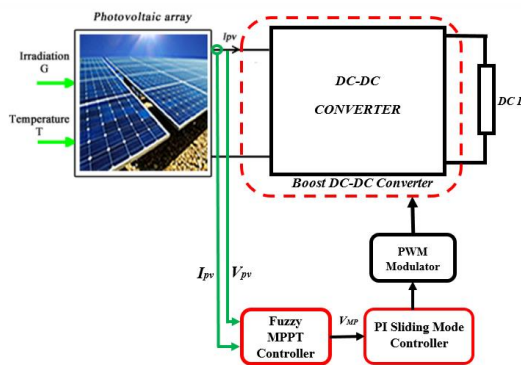


Figure 1. The complete PV system with the MPPT control unit.

converter, an MPPT control unit, and a direct current (DC) load.

### B. Characteristics of PV Array

#### 1) Model of PV panel

The photovoltaic (PV) module employs the single-diode model. The PV cell modeling utilizes the one-diode equivalent circuit illustrated in Figure 2 [13][14].

The PV cell model comprises a current source, two resistors, and a diode, as illustrated in Figure 2. The series resistance  $R_s$  is disregarded due to its very low value, and the parallel resistance  $R_p$  is also omitted due to its high resistance. Neglecting these two parameters simplifies the modeling process without compromising accuracy [15]. Equations (1)–(5) give the mathematical model of the photovoltaic cell [16]–[19]:

$$I = N_p I - N_p I_0 \left[ e^{\left( \frac{qV}{N_s A K T} \right)} - 1 \right] \quad (1)$$

The inverse saturation current  $I_0$  is:

$$I_0 = I_{0r} \left( \frac{T}{T_r} \right)^3 e^{\left( \frac{qE_g}{KA} \left( \frac{1}{T_r} - \frac{1}{T} \right) \right)} \quad (2)$$

The inverse saturation current at  $T_r$  is

$$I_{0r} = \frac{I_{scr}}{e^{\left( \frac{qV_{oc}}{N_s A K T} \right)} - 1} \quad (3)$$

Generated photocurrent is

$$I_r = \left[ I_{scr} + (K_i (T - T_r)) \right] \frac{E}{1000} \quad (4)$$

The PV module power ( $P_{pv}$ ) can therefore be obtained as follows:

$$P_{pv} = IV = N_p I_r V - N_p I_0 V \left[ e^{\left( \frac{qV}{N_s A K T} \right)} - 1 \right] \quad (5)$$

Figure 3 demonstrates the impact of irradiation on the power-voltage (P-V) curves. Hence, employing a control command to track the maximum power of the photovoltaic generators becomes essential. In this study, the MSX-60.5 panel is used. Table 1 presents the specifications of the studied PV System.

#### 2) DC-DC Converter

The dynamic equations of the boost converter of the Figure 4 are determined using (6) [12].

$$\begin{cases} \frac{di_L}{dt} = \frac{V_e - V_S}{L} - \frac{V_S}{L} u \\ \frac{dV_S}{dt} = -\frac{V_S}{RC} + \frac{i_L}{C} - \frac{i_L}{C} u \end{cases} \quad (6)$$

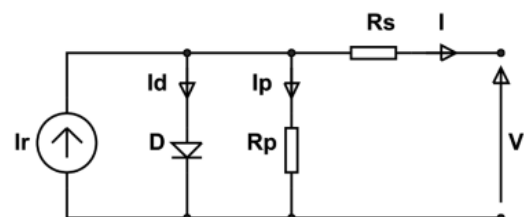


Figure 2. PV cell equivalent circuit.

TABLE 1  
SPECIFICATIONS OF PV SYSTEM

Parameter	Name	Value
$P_{max}$	Maximum power	1200 W
$V_{mpp}$	Optimum operating voltage	170.1 V
$I_{mpp}$	Optimum operating current	7.6 A
$V_{oc}$	Open circuit voltage	210.1- V
$I_{sc}$	Short-circuit current	7.8 A

## C. Methods

### 1) Proposed control

The control scheme employs a dual control loop concept: fuzzy logic is used to generate the voltage reference, and SMC is applied to generate the duty cycle  $d$  for the boost converter. SMC guides the system's state trajectory towards the sliding surface, where appropriate switching logic induces oscillations on both sides until convergence towards the equilibrium point situated on this surface.

### 2) Definition of the Sliding Surface

The sliding surface is established according to the control objectives of the system [20]. These objectives are designed to minimize the error between the measured variable and the reference to zero. The sliding surface is characterized by the voltage error ( $e_v$ ) and the current error ( $e_i$ ):

$$e_v = v_{pv} - v_{pv,ref} \quad (7)$$

$$e_i = i_{L,ref} - i_L \quad (8)$$

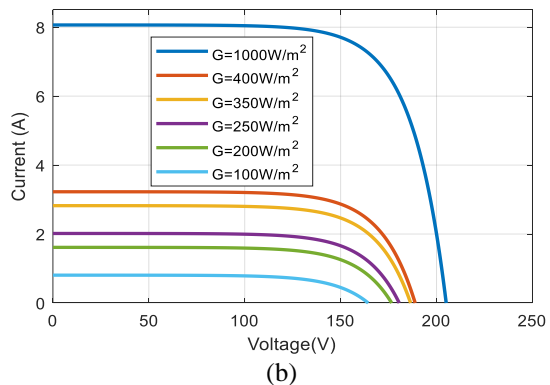
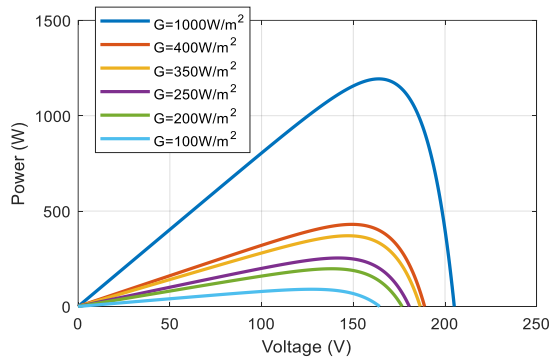


Figure 3. Influence of low irradiation on the (a) P-V and (b) I-V curves.

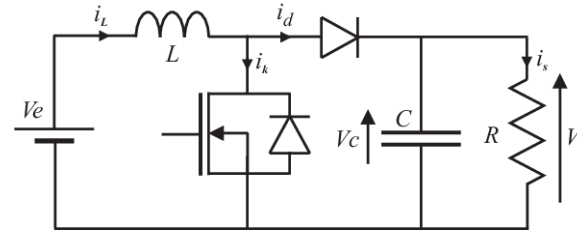


Figure 4. Boost converter.

By incorporating the derivatives of the errors defined in (7) and (8), we improve the dynamic response of the controller, thereby obtaining the set of sliding surfaces  $S$  as indicated in (9).

$$S = \begin{bmatrix} s_1 \\ s_2 \end{bmatrix} = \begin{bmatrix} e_v + k_v \frac{de_v}{dt} \\ e_i + k_i \frac{de_i}{dt} \end{bmatrix} \quad (9)$$

The constants  $k_v$  and  $k_i$  are determined according to the desired system dynamics. The choice of these gains is crucial; too small gains cause a very long response time, and too large gains generate strong oscillations at the control unit level. These oscillations can excite neglected dynamics (chattering phenomenon) or even deteriorate the control unit [21]. The use of the sign function in the control law ensures that the error converges asymptotically towards zero. However, this discontinuous function causes the problem of reticence. To address this issue, we apply the boundary layer solution, which involves performing a continuous approximation of the discontinuities present in the control law in the vicinity of the sliding surface [15]. The sign function is approximated by the hyperbolic tangent function. To reduce the effect of this phenomenon, we propose replacing the sign function with another function called a hyperbolic tangent. The control laws for the two control loops correspond to (10) and (11) [22].

$$i_{L,ref} = \left( k_{pv} + \frac{k_{iv}}{s} \right) \tanh(S_1) \quad (10)$$

$$d = \left( k_{pc} + \frac{k_{ic}}{s} \right) \tanh(S_2) \quad (11)$$

Where  $k_{pv}$ ,  $k_{iv}$ ,  $k_{pc}$  and  $k_{ic}$  are the gains of an integral proportional controller (PI),  $S_1$  and  $S_2$  are presented in (9).

### 3) Design of fuzzy logic (FLC)

Fuzzy logic control provides the advantage of being a robust control method that does not demand precise knowledge of the mathematical model of the system. Therefore, it is better suited for non-linear systems. This algorithm operates in three blocks, as shown in Figure 5: fuzzification, inference, and defuzzification. Fuzzification converts physical input variables into fuzzy sets. The input variables corresponding to the E error and the variation of the CE error are defined using (12) and (13).

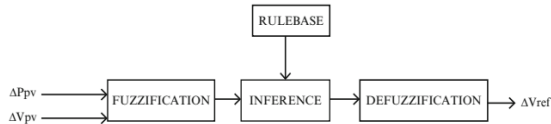


Figure 5. Block diagram of the FLC.

$$E = \frac{P(k) - P(k-1)}{I(k) - I(k-1)} \quad (12)$$

$$CE = E(k) - E(k-1) \quad (13)$$

In our case, the inputs of the fuzzy controller are the variation of the power ( $\Delta P_{pv}$ ) and the variation of the voltage ( $\Delta V_{pv}$ ) of the PV generator. The output corresponds to the reference voltage variation ( $\Delta V_{ref}$ ), as shown in Figure 6. The following linguistic variables are therefore assigned to these quantities: PL (Positive Large), PM (Positive Medium), PS (Positive Small), Z (Zero), NS (Negative Small), NM (Negative Medium) and NL (Negative Large).

In the inference stage, decisions are made by establishing logical relationships between the inputs and the output while defining the membership rules. The inference rules are then formulated in Table 2. Finally, during the defuzzification process, the fuzzy output subsets are converted into numerical values. Figure 7 is the surface representation of the membership functions for the fuzzy model.

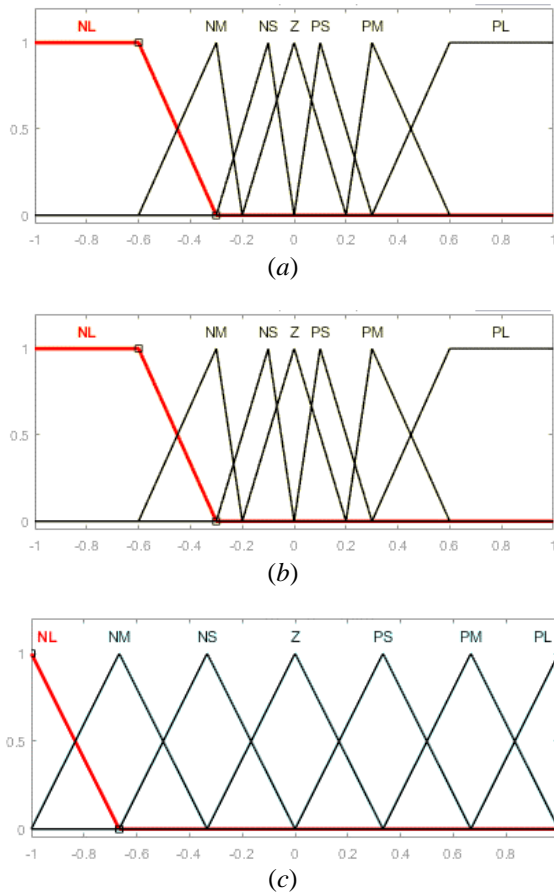

 Figure 6. Membership functions for the fuzzy model (a) input  $\Delta P_{pv}$ , (b) Input  $\Delta V_{pv}$  (c) output  $\Delta V_{ref}$ .

 TABLE 2  
 RULE BASE FOR THE FUZZY MODEL

$\Delta V_{pv}$	$\Delta P_{pv}$						
	NL	NM	NS	Z	PS	PM	PL
NL	PL	PL	PL	PL	NM	Z	Z
NM	PL	PL	PL	PM	PS	Z	Z
NS	PL	PM	PS	PS	PS	Z	Z
Z	PL	PM	PS	Z	NS	NM	NL
PS	Z	Z	NM	NS	NS	NM	NL
PM	Z	Z	NS	NM	NL	NL	NL
PL	Z	Z	NM	NL	NL	NL	NL

#### 4) Particle swarm optimization algorithm

The PSO (particle swarm optimization) algorithm was initially developed by Kennedy and R. Eberhart [23]. It is an iterative algorithm belonging to the category of evolutionary stochastic methods with rapid convergence. Numerous applications of this algorithm in various fields, particularly in engineering, have demonstrated its superiority over other stochastic methods such as ant colony optimization, biogeography, and genetic algorithms. At each computational step, individual values are compared based on the objective function, and new guides are selected. During its execution, the algorithm proceeds through the steps outlined in the flowchart depicted in Figure 8. The position and velocity of each particle are updated using (14).

$$\begin{cases} V_{i+1} = \gamma_1 V_i + \gamma_2 (x_{ip} - x_i) + \gamma_p (x_g - x_i) \\ x_{i+1} = x_i + V_{i+1} \end{cases} \quad (14)$$

With  $\gamma_1, \gamma_2, \gamma_p \in [0, 1]$ ,  $x_{ip}$  et  $x_g$ , respectively, represent the best position of the  $i$ th particle from the first iteration and the best global position of the entire swarm.  $V_i$  is the velocity of each particle.

The PSO optimization algorithm's task is to calculate the gain  $K_1, K_2, K_3$  for fuzzy logic,  $k_v, k_i$  for sliding mode, and  $k_{pv}, k_{iv}, k_{pc}$ , and  $k_{ic}$  for two PI that minimize the criterion  $J$  from iteration to iteration. In total, nine variables must be set for each control loop. As a result, we have nine objective functions, each of which is the minimization of the absolute integral of the error determined by (15).

$$J_{ITAE} = \int_0^{t_{simul}} |e_s| dt \quad (15)$$

Where  $t_{simul}$  is the simulation time and  $e_s$  is the error between a reference state and its measurement. In order

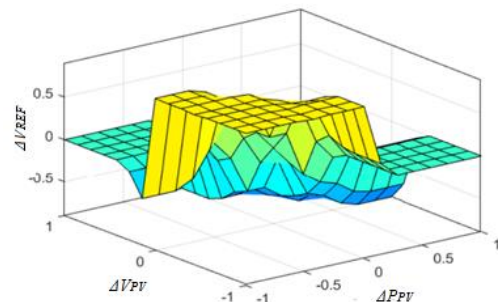


Figure 7. Rules of fuzzy logic on the surface.

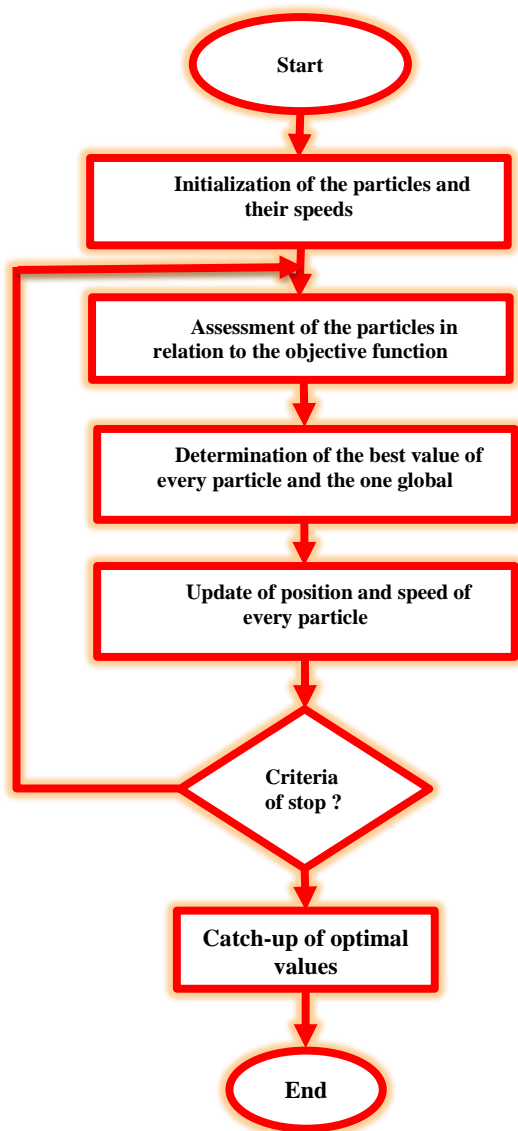


Figure 8. flowchart of the PSO algorithm.

to avoid the use of multi-objective optimization techniques, the formulation of a single objective function is carried out using the weighting method. Equation (16) formulate the global objective function.

$$J = \sum_{i=1}^9 \alpha_i J_i \tag{16}$$

With:

$$\alpha_1 + \alpha_2 + \alpha_3 + \alpha_4 + \alpha_5 + \alpha_6 + \alpha_7 + \alpha_8 + \alpha_9 = 1.$$

Indeed, at each iteration, the algorithm seeks a better compromise between the different gains in order to minimize the objective function. Figure 9 shows the small variation of the objective function.

The selection of these parameters directly impacts the controller's performance. Properly configuring these variables leads to a stable and robust response. In this article, the PSO is employed to compute these parameters.

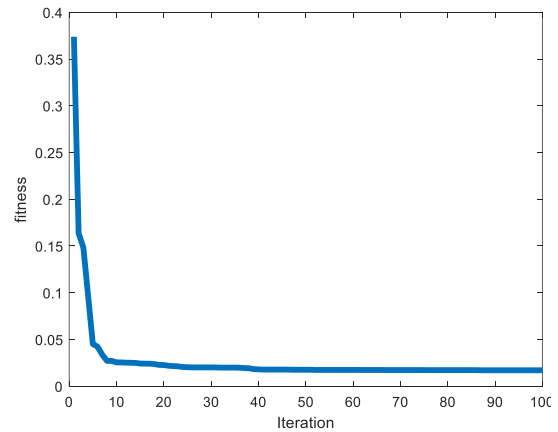


Figure 9. Evolution of the objective function.

Figure 10 shows the overall system, which is divided into four blocks, namely the three-block control and the DC-DC converter block. The PSO algorithm is utilized in all control blocks to compute optimal gains.

### III. RESULTS AND DISCUSSION

The gains obtained by applying the PSO algorithm are provided in Table 3. The tests involve simulations of hard, medium, and soft insolation variations, increasing and decreasing, under low irradiation conditions. Two specific cases were taken into account for the tests; they are hard variation involves rapid and substantial insolation changes (400 W/m<sup>2</sup>) with abrupt transitions, and the other one is middle variation, this scenario features rapid and moderate insolation changes (100 W/m<sup>2</sup>) with sharp transitions.

According to Figure 11, for low irradiancies, i.e., from 100 W/m<sup>2</sup> to 400W/m<sup>2</sup> at varied temperatures (between 20 °C and 40 °C), the proposed algorithm registers excellent performance in terms of monitoring and transient response. No overshoot is observed during the variation of the sunshine for the proposed Fuzzy-SMC algorithm. The proposed MPPT algorithm demonstrates a substantial improvement in terms of response time, particularly during periods of rapidly

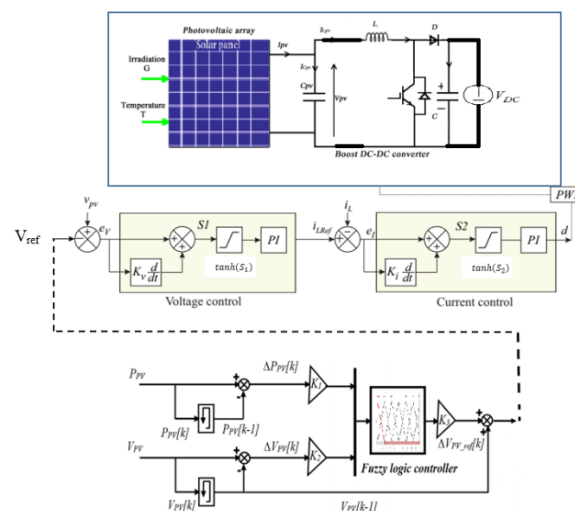


Figure 10. Block diagram of the system.

TABLE 3  
 VALUE OF GAINS

Parameter	Value of Gains
$K1$	41.66
$K2$	33.99
$K3$	24.02
$k_p$	151.04
$k_i$	863.37
$k_{pv}$	18.97
$k_{iv}$	55.34
$k_{pc}$	50.34
$k_{ic}$	21.15

changing atmospheric conditions. Specifically, it achieves a response time of 26 ms, whereas the P&O method requires 76 ms. Additionally, the proposed algorithm exhibits excellent performance in a steady state, with no ripple or oscillation around the MPP, a feature lacking in the conventional P&O algorithm, which shows fluctuations between 0.3 and 1 W.

Furthermore, referring to Figure 11, it is observed that the temperature does not significantly impact the power output as long as it remains within an acceptable range for an irradiance of 400 W/m<sup>2</sup>.

By comparing the values in Table 4 with the characteristics in Figure 3, we also confirm that our algorithm displays a better yield in terms of attainment of the MPPT point. For example, for a low irradiation value equal to 400 W/m<sup>2</sup>, the corresponding MPP is 497.4 W. Our algorithm reaches 274.2 W against 229.2 W for P&O, a gain in power of 45 W, which proves the superiority of our algorithm in low irradiation. Our algorithm is, therefore, better suited for regions with low irradiation.

Figure 12 presents simulation results of the system

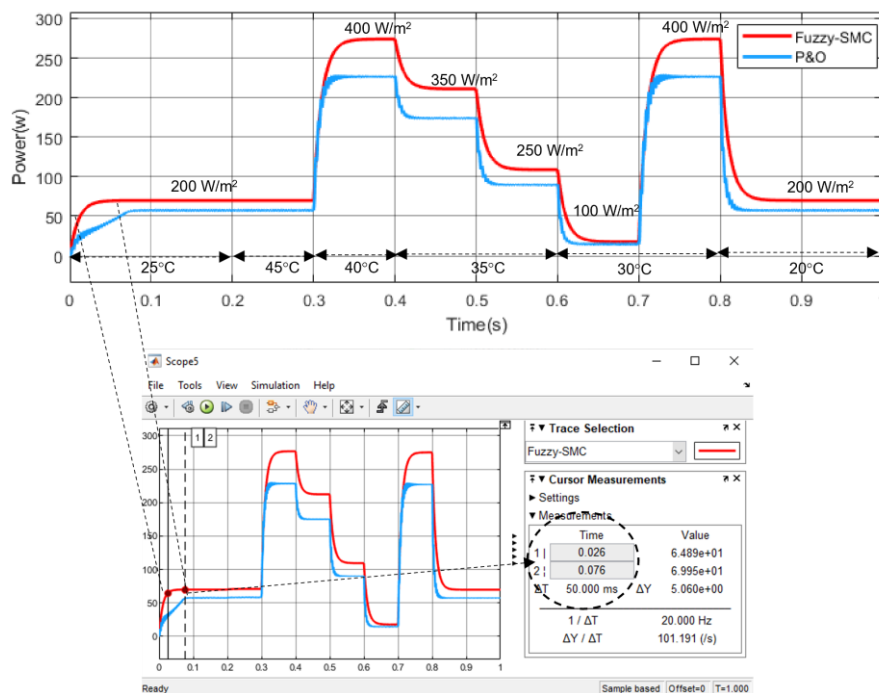


Figure 11. The output power under low irradiation and variable temperature.

for constant irradiation of 800 W/m<sup>2</sup>, with temperature

 TABLE 4  
 RESULTS COMPARISON

Irradiation	MPP (w)	Max Power (w)		Ripple (w)	
		P&O	fuzzy-SMC	P&O	fuzzy-SMC
400 W/m <sup>2</sup>	497.4	229.2	274.2	0.3	NO
350 W/m <sup>2</sup>	435.2	174.5	211	1	NO
250 W/m <sup>2</sup>	310.1	89.9	108.8	0.6	NO
200 W/m <sup>2</sup>	247.2	57.7	69.983	0.3	NO
100 W/m <sup>2</sup>	121.5	14.5	17.67	0.1	NO

varying in increasing time, i.e., 25 °C in the interval [0; 0.2], 45 °C in the interval [0.2; 0.3], and then decreasing, i.e., 40 °C in the interval [0.3; 0.4], 35 °C in the interval [0.4; 0.6], 30 °C in the interval [0.6; 0.8], and finally 20 °C in the interval [0.8; 1]. It is evident to note that when irradiation reaches 800 W/m<sup>2</sup>, temperature variations significantly influence the power. We immediately observe that when the temperature rises to 45 °C, the output power of the fuzzy-SMC system decreases significantly, although it remains higher than that of the P&O system. Similarly, when the temperature decreases to its lowest level, i.e., 20 °C, the power of the fuzzy-SMC system increases considerably. Whether the temperature increases or decreases, the developed system remains effective for low irradiance levels compared to the P&O system.

In Figure 13, the change in solar irradiance is assumed to follow a trapezoidal pattern with a temperature variation between 20 °C and 45 °C to validate the proper functioning of the proposed method. It should be noted, however, that 800 W/m<sup>2</sup> is the permanently permissible irradiation value in the sizing of the solar system. We observe that the output power

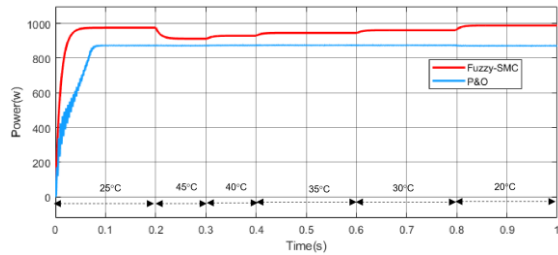


Figure 12. The output power under low constant irradiation (800 W/m<sup>2</sup>) and variable temperature.

evolves normally and is not affected by the temperature variation.

Figures 11, 12, and 13 illustrate the outcomes achieved through the proposed algorithm, juxtaposed with those obtained using the P&O algorithm. Based on these results, it can be deduced that the proposed fuzzy-SMC algorithm displays a notable enhancement in tracking the Maximum Power Point (MPP) during periods of low irradiation. In contrast to the traditional (P&O) algorithm, the proposed fuzzy-SMC approach effectively minimizes oscillations around the maximum power and precisely tracks the MPP. This precision directly influences energy conservation, mitigating energy loss. Figure 11 demonstrates that the designed system remains robust against temperature variations as long as the irradiation does not exceed 400 W/m<sup>2</sup>. Figure 12 shows that when the irradiation increases to 800 W/m<sup>2</sup>, the effect of temperature variation, exceeding 35°C becomes noticeable. However, it is noteworthy that when the temperature drops below 25 °C, the power gain increases significantly, representing a considerable advantage over the P&O method. This demonstrates that the system responds effectively to temperature variations.

TABLE 5  
RESULTS COMPARISON

Algorithm	P&O	Fuzzy-SMC
Tracking Speed	0.76s	0.026s
Extracted Energy Efficiency in low irradiation (%) 800w/m <sup>2</sup>	89.08	94.89
Steady State oscillation (% of power)	High	Less
Accuracy	Low	Highest
Complexity	Easy	Medium

Based on the test results, it can be concluded that the key contributions of the proposed Fuzzy-SMC algorithm include the reduction of ripple and elimination of overshoot, improved response time, and its ability to operate effectively under low irradiation, particularly in swiftly changing environmental conditions. These enhancements lead to an overall reduction in energy losses. Table 5 provides a comparison of two MPPT algorithms for the considered scenario.

#### IV. CONCLUSION

In this study, the MPPT technique was developed to improve the control of photovoltaic systems in case of low irradiation. This command takes into account random changes in atmospheric conditions in regions with low irradiation. The simulation results unequivocally showcased the efficacy of this approach, highlighting its performance in terms of response speed, robustness, and accuracy in tracking the MPP under variable and non-uniform low irradiation weather conditions. Indeed, for different levels of low irradiation, the system showed superior performance with energy savings of up to 70 W, which is significant, with an increased speed of up to 0.026 s.

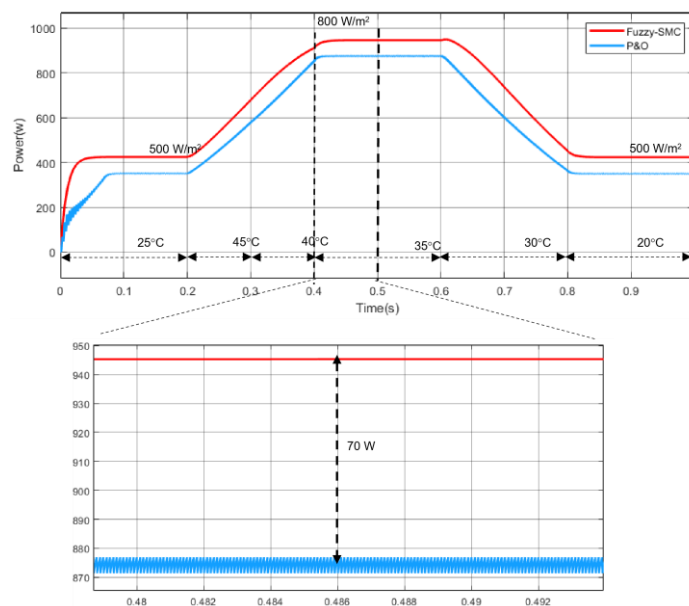


Figure 13. The power obtained by the suggested algorithm using the trapezoidal form of solar irradiation with variable temperature.

## DECLARATIONS

### Conflict of Interest

The authors have declared that no competing interests exist.

### CRedit Authorship Contribution

Dieudonné Marcel Djanssou: Conceptualization, Methodology, Software, Visualization, Investigation, Writing-Original draft preparation Writing-Reviewing and Editing; Abdouramani Dadjé: Data curation, Writing-Reviewing and Editing; Fabrice Kwefu Mbakop: Data curation, Reviewing and Editing, Noël Djongyang: Data curation, Supervision, Funding Acquisition.

### Funding

The author(s) received no financial support for the research, authorship, and/or publication of this article.

## REFERENCES

- [1] R. Signerski, "Effect of band gap on power conversion efficiency of single-junction semiconductor photovoltaic cells under white light phosphor-based LED illumination," *Mater. Sci. Semicond. Process.*, vol. 107, Mar. 2020, Art. no. 104812, doi: 10.1016/j.mssp.2019.104812.
- [2] S. Sumathi, L. Ashok Kumar, and P. Surekha, *Solar PV and Wind Energy Conversion Systems: An Introduction to Theory, Modeling with MATLAB/SIMULINK, and the Role of Soft Computing Techniques*, Springer Cham, 2015.
- [3] M. Kermadi and E. M. Berkouk, "Artificial intelligence-based maximum power point tracking controllers for photovoltaic systems: comparative study," *Renew. Sustain. Energy Rev.*, vol. 69, Feb. 2016, pp. 369–386, 2017, doi: 10.1016/j.rser.2016.11.125.
- [4] A. Dadjé, N. Djongyang, J. D. Kana, and R. Tchinda, "Maximum power point tracking methods for photovoltaic systems operating under partially shaded or rapidly variable insolation conditions: a review paper," *Int. J. Sustain. Eng.*, vol. 9, no. 4, pp. 224–239, Feb. 2016, doi: 10.1080/19397038.2016.1149525.
- [5] M. Premkumar and R. Sowmya, "An effective maximum power point tracker for partially shaded solar photovoltaic systems," *Energy Rep.*, vol. 5, pp. 1445–1462, Nov. 2019, doi: 10.1016/j.egy.2019.10.006.
- [6] S. Mohanty, B. Subudhi, and P. K. Ray, "A new MPPT design using grey wolf optimization technique for photovoltaic system under partial shading conditions," *IEEE Trans. Sustain. Energy*, vol. 7, no. 1, pp. 181–188, Jan. 2016, doi: 10.1109/TSSTE.2015.2482120.
- [7] C. Huang, L. Wang, R. S. C. Yeung, Z. Zhang, H. S. H. Chung, and A. Bensoussan, "A prediction model-guided jaya algorithm for the PV system maximum power point tracking," *IEEE Trans. Sustain. Energy*, vol. 9, no. 1, pp. 45–55, Jan. 2018, doi: 10.1109/TSSTE.2017.2714705.
- [8] A. Badis, M. N. Mansouri, and M. H. Boujmil, "A genetic algorithm optimized MPPT controller for a PV system with DC-DC boost converter," in *Proc. 2017 Int. Conf. Eng. MIS, ICEMIS 2017*, Monastir, Tunisia, 2017, pp. 1–6, doi: 10.1109/ICEMIS.2017.8273010.
- [9] A. S. Benyoucef, A. Chouder, K. Kara, S. Silvestre, and O. A. Sahed, "Artificial bee colony based algorithm for maximum power point tracking (MPPT) for PV systems operating under partial shaded conditions," *Appl. Soft Comput. J.*, vol. 32, pp. 38–48, Jul. 2015, doi: 10.1016/j.asoc.2015.03.047.
- [10] A. E. Khateb, N. A. Rahim, J. Selvaraj, and M. N. Uddin, "Fuzzy logic controller based sepic converter of maximum power point tracking," in *Proc. IEEE Ind. Appl. Soc. Annu. Meet.*, Las Vegas, NV, USA, 2012, pp. 1–9, doi: 10.1109/IAS.2012.6374024.
- [11] J. Ahmed and Z. Salam, "A critical evaluation on maximum power point tracking methods for partial shading in pv systems," *Renew. Sustain. Energy Rev.*, vol. 47, pp. 933–953, Jul. 2015, doi: 10.1016/j.rser.2015.03.080.
- [12] D. M. Djanssou, A. Dadjé, A. Tom, and N. Djongyang, "Improvement of the dynamic response of robust sliding mode MPPT controller-based PSO algorithm for PV systems under fast-changing atmospheric conditions," *Int. J. Photoenergy*, vol. 2021, Jun. 2021, Art. no. 6671133, doi: 10.1155/2021/6671133.
- [13] A. Dadjé *et al.*, "Modified social network search algorithm combined with Halley's method for parameter estimation in a photovoltaic cell, module, and array," *J. Sol. Energy Res.*, vol. 8, no. 2, pp. 1484–1496, Apr. 2023, doi: 10.22059/jser.2023.357161.1287.
- [14] D. M. Djanssou, A. Dadjé, and N. Djongyang, "Estimation of photovoltaic cell parameters using the honey badger algorithm," *Int. J. Eng. Adv. Technol.*, vol. 11, no. 5, pp. 109–124, Jun. 2022, doi: 10.35940/ijeat.e3552.0611522.
- [15] H. Yatimi and E. Aroudam, "Assessment and control of a photovoltaic energy storage system based on the robust sliding mode mppt controller," *Sol. Energy*, vol. 139, pp. 557–568, Dec. 2016, doi: 10.1016/j.solener.2016.10.038.
- [16] A. Dadjé, F. K. Mbakop, D. M. Djanssou, and R. Z. Falama, "Modeling the behavior of a photovoltaic generator using a four-parameter electrical model 2 . modeling the photovoltaic generator using a four-parameter electrical model," *Eng. Phys.*, vol. 6, no. 1, pp. 5–12, 2022, doi: 10.11648/j.ep.20220601.12.
- [17] Y. A. Mindzie, J. Kenfack, V. Joseph, U. Nzotcha, D. M. Djanssou, and R. Mbounguen, "Dynamic performance improvement using model reference adaptive control of photovoltaic systems under fast-changing atmospheric conditions," *Int. J. Photoenergy*, vol. 2023, 2023, doi: 10.1155/2023/5703727.
- [18] M. Kumar and A. Kumar, "An efficient parameters extraction technique of photovoltaic models for performance assessment," *Sol. Energy*, vol. 158, pp. 192–206, Dec. 2017, doi: 10.1016/j.solener.2017.09.046.
- [19] J. Bai, S. Liu, Y. Hao, Z. Zhang, M. Jiang, and Y. Zhang, "Development of a new compound method to extract the five parameters of pv modules," *Energy Convers. Manag.*, vol. 79, pp. 294–303, Mar. 2014, doi: 10.1016/j.enconman.2013.12.041.
- [20] C. C. Ahmed, M. Cherkaoui, and M. Mokhlis, "MPPT control for photovoltaic system using hybrid method under variant weather condition," in *Proc. 2019 Int. Conf. Wirel. Technol. Embed. Intell. Syst. (WITS 2019)*, Fez, Morocco, pp. 1–5, 2019, doi: 10.1109/WITS.2019.8723854.
- [21] M. R. Mojallizadeh, M. Badamchizadeh, S. Khanmohammadi, and M. Sabahi, "Designing a new robust sliding mode controller for maximum power point tracking of photovoltaic cells," *Sol. Energy*, vol. 132, pp. 538–546, Jul. 2016, doi: 10.1016/j.solener.2016.03.038.
- [22] C. Lascu, I. Boldea, and F. Blaabjerg, "Direct torque control of sensorless induction motor drives: a sliding-mode approach," *IEEE Trans. Ind. Appl.*, vol. 40, no. 2, pp. 582–590, Mar. 2004, doi: 10.1109/TIA.2004.824441.
- [23] M. O. Okwu and L. K. Tartibu, "Particle swarm optimisation," *Metaheuristic Optimization: Nature-Inspired Algorithms Swarm and Computational Intelligence, Theory and Applications*, Springer Cham, 2021, doi: 10.1007/978-3-030-61111-8\_2.